Coherent Raman scattering imaging of lipid metabolism in cancer

Shuo Zhang[*], Yexuan He[*] and Shuhua Yue[*,†,‡]

[*]Key Laboratory of Biomechanics and
Mechanobiology (Beihang University),
Ministry of Education, Institute of Medical Photonics,
Beijing Advanced Innovation Center for Biomedical Engineering,
School of Biological Science and Medical Engineering,
Beihang University, Beijing 100083, P. R. China

[†]MoE Key Laboratory for Biomedical Photonics,
Wuhan National Laboratory for Optoelectronics-Huazhong
University of Science and Technology,
Wuhan 430074, P. R. China
[‡]yue_shuhua@buaa.edu.cn

Cancer cells dysregulate lipid metabolism to accelerate energy production and biomolecule synthesis for rapid growth. Lipid metabolism is highly dynamic and intrinsically heterogeneous at the single cell level. Although fluorescence microscopy has been commonly used for cancer research, bulky fluorescent probes can hardly label small lipid molecules without perturbing their biological activities. Such a challenge can be overcome by coherent Raman scattering (CRS) microscopy, which is capable of chemically selective, highly sensitive, submicron resolution and high-speed imaging of lipid molecules in single live cells without any labeling. Recently developed hyperspectral and multiplex CRS microscopy enables quantitative mapping of various lipid metabolites in situ. Further incorporation of CRS microscopy with Raman tags greatly increases molecular selectivity based on the distinct Raman peaks well separated from the endogenous cellular background. Owing to these unique advantages, CRS microscopy sheds new insights into the role of lipid metabolism in cancer development and progression. This review focuses on the latest applications of CRS microscopy in the study of lipid metabolism in cancer.

Keywords: Coherent Raman scattering microscopy; cancer metabolism; lipid metabolism.

[‡]Corresponding author.

1. Introduction

Reprogramming of lipid metabolism has become a well-known hallmark of human cancers.[1,2] Tumor cells exhibit high rates of lipid metabolic pathways for energy production, structural components of cellular membranes and signaling messengers for rapid survival, proliferation and respondence to cancer therapy. The dysregulated metabolic pathways are adjusted accordingly, which involves the process of lipid synthesis, uptake, storage and lipolysis.[3,4] Endogenous lipid biosynthesis is increased to promote cancer progression by upregulating the fatty acid (FA) biosynthetic enzymes, such as acetyl-CoA carboxylase (ACC), ATP citrate lyase (ACLY) and fatty acid synthase (FASN),[5] and the mevalonate pathway for *de novo* cholesterol synthesis.[6] Stearoyl-CoA desaturase (SCD), the principal enzyme responsible for catalyzing FA desaturation, has been reported to protect cancer from lipotoxicity for cell survival.[7] A stronger capacity of exogenous lipid uptake has been recognized in cancer cells, accompanied by upregulated levels of transporters in the plasma membrane, such as FA translocase (FAT/CD36), FA transport proteins (FATPs), FA binding proteins (FABPs) and lipoprotein receptors.[8] In parallel, multiple lipases involved in lipid degradation and β-oxidation, are necessary for rapid proliferation and metastasis of cancer cells.[9,10] Moreover, excess triglyceride (TG) and cholesteryl ester (CE) storage in the lipid droplet (LD), a highly dynamic organelle, has been commonly seen in various types of human cancers.[11] A more comprehensive understanding of lipid metabolic reprogramming has contributed to new strategies of cancer treatment.[12,13]

It's noticeable that lipid metabolism in cancer is highly dynamic and intrinsically heterogeneous.

Conventionally, biospecimens are broken into homogenates and then analyzed by chemical assays, nuclear magnetic resonance (NMR) spectroscopy or mass spectrometry (MS), to identify lipid species and their concentrations. However, these methods lack spatial and temporal information at the cellular level.[14–16] Recently, mass spectrometry imaging (MSI) has been advanced to analyze both lipid distribution and composition *in situ*, but it is intrinsically sample-destructive with limited spatial resolution, which hinders subcellular *in situ* analysis and live cell measurement.[17] Although fluorescence microscopy can offer live imaging of lipid distribution in single cells, fluorescent lipid probes are so bulky that likely interfere with the metabolic activities of lipids. Moreover, fluorescence detection is also affected by photobleaching and autofluorescence. Furthermore, it also fundamentally limited by the broad fluorescent spectra, in which case, just a limited kind of molecules can be labeled simultaneously because of the associated "color barrier".[18] Thus, in order to promote the understanding of lipid metabolism in cancer, there is a need for a label-free chemical-selective imaging technique with high temporal and spatial resolution.

With characteristics of high chemical selectivity and label-free imaging, Raman scattering microscopy is desirable for lipid research.[19] Unfortunately, the cross-section of spontaneous Raman scattering (shown in Fig. 1) is extremely small ($\sim 10^{-30}\,\text{cm}^2$ per molecule),[20] in which case, it takes about tens of minutes per frame of $\sim 240 \times 100$ pixels and its application of capturing the dynamics in living systems was limited.[21] As one way to enhance the Raman scattering signal, coherent Raman scattering (CRS) uses pulse lasers with different
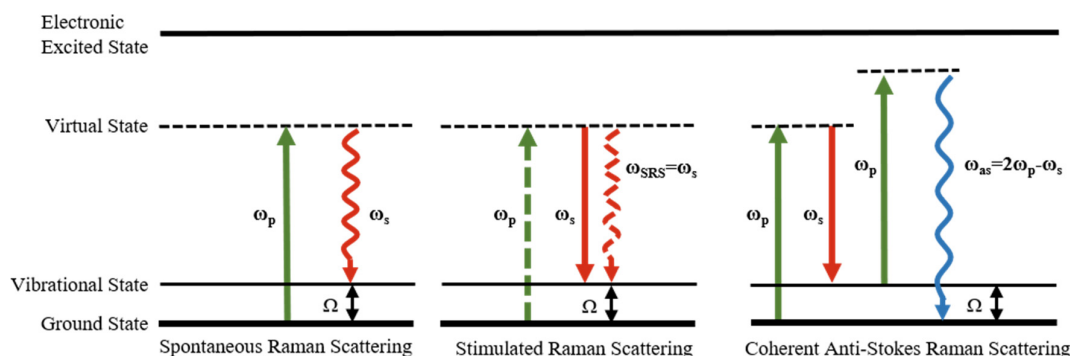

Fig. 1. Energy diagram of spontaneous Raman scattering, SRS and coherent anti-Stokes Raman scattering (CARS).

frequencies, that is pump (ω_p) and Stokes (ω_s). When the frequency difference between two excitation fields $(\omega_p. - \omega_s)$ is tuned to match the vibrational frequency of targeted chemical bonds, the rate of vibrational transition is greatly amplified by about 10^{6-8} times and the Raman scattering signal can be remarkably boosted, which permits high speed imaging of biomolecules in living systems.[22,23] There are four simultaneous CRS processes: stimulated Raman gain (SRG) and stimulated Raman loss (SRL) (which both belong to stimulated Raman scattering (SRS)), coherent Stokes Raman scattering (CSRS) at the frequency of $\omega_s - (\omega_p - \omega_s)$ and coherent anti-Stokes Raman scattering (CARS) at the frequency of $(\omega_p - \omega_s) + \omega_p$.[19,24,25] Compared to CARS, SRS is not disturbed by nonresonant background. Meanwhile, SRS signal is affected by heterodyne optical processes, such as cross-phase modulations, photothermal effects and transient absorption. SRS signal is linearly dependent on the molecular concentration, while the signal in CARS is proportional to the square of its concentration.[26–28] Owing to high temporal and spatial resolution, label-free CRS microscopy has been widely used for the study of lipid metabolism in living systems.[19,29–32]

C–H bond is abundant in living cells and the detection specificity of label-free CRS imaging is usually limited because molecules with the same chemical bond will have an overlapping effect on the spectrum of detected targets, in which case, it's difficult to distinguish the specific molecule of interest. In contrast, the cell-silent Raman window $(1800–2600\,\mathrm{cm}^{-1})$, without endogenous molecules vibrate, is suitable for specific detection of interest by introducing specific chemical bonds to avoid the endogenous cellular background skillfully.[33] Various Raman tags have been developed to replace the C–H bonds by specific chemical bonds (such as carbon-deuterium (C-D) and alkyne probe (C≡C)) in molecules to track metabolic processes of specific biomolecules.[18,33,34] Unlike bulky fluorophores for fluorescence microscopy, Raman tags for CRS are much smaller in size than fluorophores, rendering less interference to the intracellular metabolism and keeping more resistance to photobleaching.[35,36] Integration of SRS microscopy with Raman tags allows visualization of cell metabolism of nucleic acids, amino acids, glucose, fatty acids and cholesterol in single cells *in vitro* and *in vivo*.[23,37–40]

In recent decades, CRS microscopy has been rapidly developed and applied in lipid research.[19,20,24,33,41] This review focuses on the latest applications of CRS imaging of lipid metabolism in cancer.

2. CRS Imaging of Intracellular Lipid Droplets (LDs) in Cancer

Intracellular LDs consist of a monolayer of phospholipid and are filled with neutral lipids, primarily TGs and CEs. As an independent and dynamic organelle, LDs stores excess FAs and cholesterol to prevent cells from potential lipotoxicity and endoplasmic reticulum stress. By regulating the balance between storage and release of various lipids, LDs are directly involved in cell processes of energy production, membrane fluidity and signaling transduction, which are essential for cell survival, growth and proliferation.[42,43] In recent years, LD accumulation has been commonly identified as a characteristic for multiple types of cancers and is associated with cancer prognosis.[44–46] The close relationship between carcinogenic pathways and LD accumulation has also been increasingly recognized, which suggests LD as a potential biomarker for cancer diagnosis and treatment.

LDs have a high density of C–H bonds and CRS imaging shows a sufficient sensitivity to LDs at $2845\,\mathrm{cm}^{-1}$,[26,47] which makes CRS a powerful technique to study the role of LDs in cancer development and progression. Cholesterol, as an essential biomolecule for cell development, plays an important role in maintaining signal transduction, membrane structure and providing precursors for hormone synthesis.[48,49] As a rate-limiting enzyme for cholesterol synthesis, squalene monooxygenase (SQLE) plays a crucial role in catalyzing the oxidation of squalene to 2,3-oxidosqualene. SRS images revealed that SQLE loss led to squalene accumulation in LDs in the cholesterol auxotrophic lymphomas.[50] As the critical enzyme is responsible for catalyzing the esterification from free cholesterol into CEs, sterol O-acyltransferase (SOAT-1) maintains intracellular cholesterol homeostasis[51] and its dysregulation has been found in many cancers, such as prostate, pancreatic, glioblastoma, lung and colon cancer.[52–58] Integrated SRS imaging and confocal Raman spectroscopy were performed to analyze LD amount and composition in human

prostate tissues (shown in Fig. 2(a)). As shown in Raman spectrum of pure cholesteryl oleate, characteristic bands for cholesterol rings at $702\,cm^{-1}$ and for ester bond at $1742\,cm^{-1}$ were also presented in cancerous tissues, but not in the normal tissues. In this case, aberrant CE accumulation was found in the cancerous tissues. Such CE accumulation was induced by the loss of tumor suppressor PTEN and
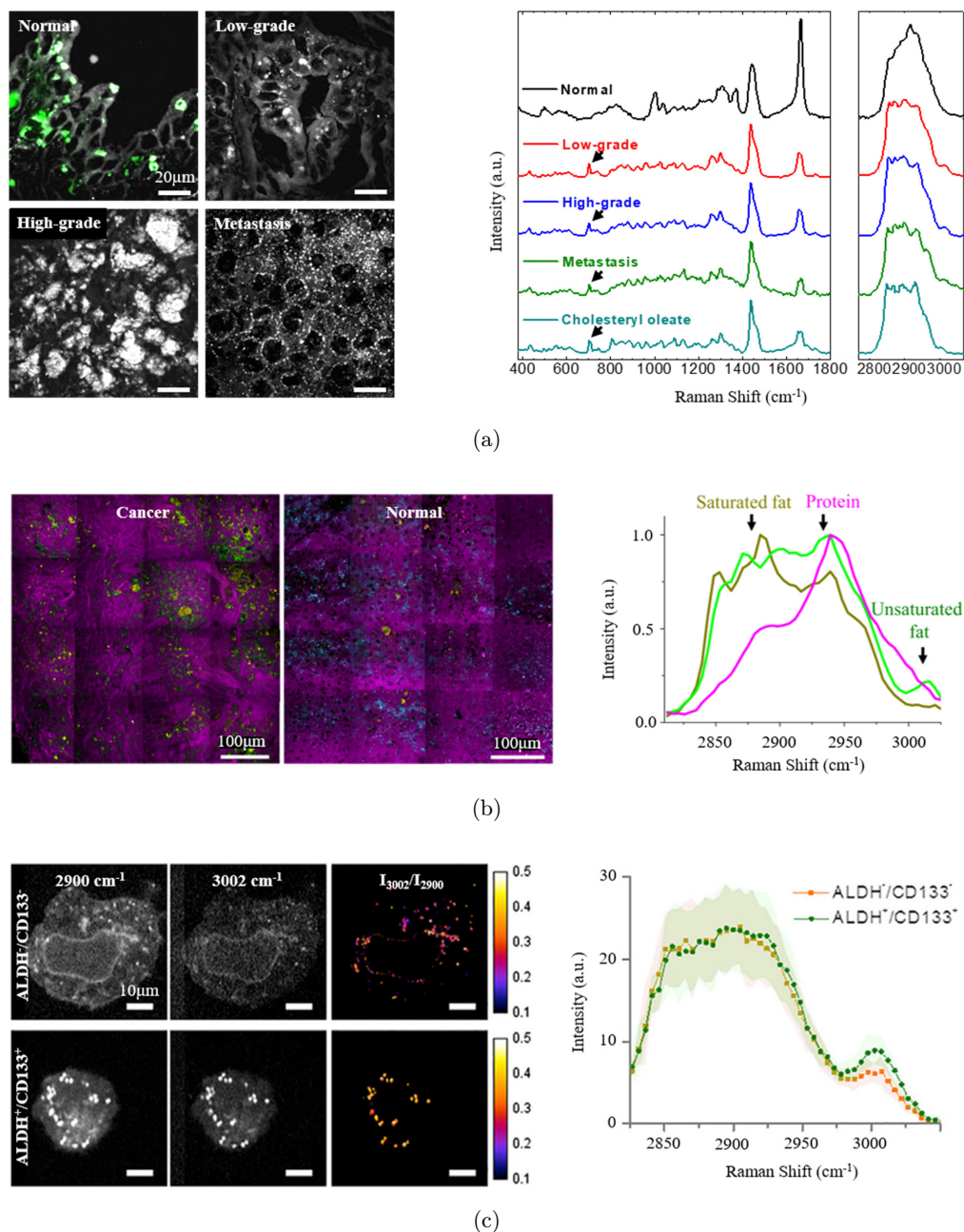

(a)

(b)

(c)

Fig. 2. SRS imaging of lipid metabolism in cancer tissues and cells. (a) Representative SRS images of normal prostate, low-grade PCa, high-grade PCa and metastatic PCa (liver) tissues, respectively. Scale bar = $20\,\mu$m. The right Raman spectra are representative of the autofluorescent granules in normal prostate, LDs in prostate cancers and pure cholesteryl oleate. Spectral intensity was normalized by CH_2 bending band at $1442\,cm^{-1}$. Black arrows indicate the characteristic bands of cholesterol rings at $702\,cm^{-1}$. Reproduced with permission from Ref. 58. (b) Large-scale hyperspectral SRS images of saturated fat (yellow), unsaturated fat (green), lipofuscin granules (cyan) and protein (magenta) in liver cancer tissues and adjacent normal tissues. Scale bar = $100\,\mu$m. Raman spectra of saturated, unsaturated lipid and protein were shown in the right corner. Reproduced with permission from Ref. 62. (c) Hyperspectral SRS images and average Raman spectra of non-CSCs (ALDH$^-$/CD133$^-$) and non-CSCs (ALDH$^+$/CD133$^+$) COV362 cells. Scale bars = $10\,\mu$m. Reproduced with permission from Ref. 63.

subsequent activation of PI3K/AKT pathway, and promoted cancer progression and metastasis.[58] In addition, by using SRS microscopy and confocal Raman spectroscopy, increased CE accumulation was also found in the pancreatic cancer tissues, but not in the normal tissues. Inhibition of cholesterol esterification with avasimibe, a specific SOAT-1 inhibitor, substantially reduced cancer cells migration and metastasis both *in vitro* and *in vivo*.[53,55] More recently, a large number of CE-rich LDs were found in the advanced melanoma. Reduced pigmentation and increased lipid accumulation occurred during the progression from low-grade to advanced melanoma.[59] In addition to regulating various cellular processes, such as growth and proliferation, SRS imaging revealed CE accumulation in drug-resistant cancer cells, including gemcitabine-resistant pancreatic ductal adenocarcinoma (PDAC) and imatinib-resistant chronic myelogenous leukemia (CML).[60,61]
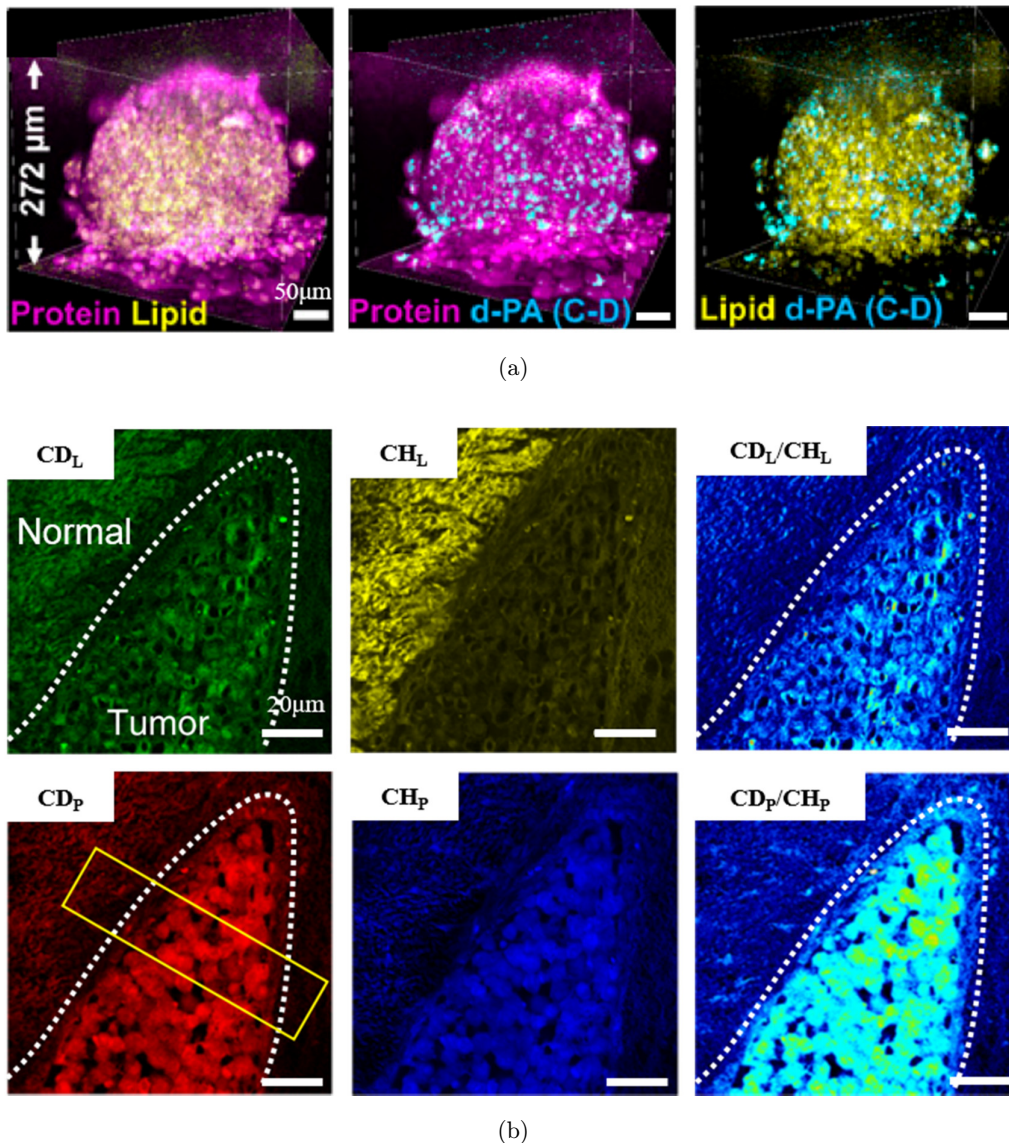

(a)

(b)

Fig. 3. Raman-tagged SRS imaging of lipid metabolism in cancer. (a) Clearing-enhanced SRS images of proteins (magenta), preexisting lipids (yellow) and newly synthesized LDs after d-PA treatment (cyan) in 3D tumor spheroids of breast cancer at the depth of $22\,\mu$m and $200\,\mu$m. Scale bar $= 50\,\mu$m. Reproduced with permission from Ref. 66. (b) DO-SRS images (combination deuterium oxide probing and SRS) at the channels of CD_L ($2135\,cm^{-1}$), CH_L ($2846\,cm^{-1}$), CD_P ($2185\,cm^{-1}$), CH_P ($2940\,cm^{-1}$) and ratio image (CD_L/CH_L, CD_P/CH_P) in the brain slices *ex vivo* from a glioblastoma mouse drank 25% D_2O for 15 days. There was a contrast boundary between glioblastoma and normal brain tissues (white dashed line). Scale bar $= 20\,\mu$m. Reproduced with permission from Ref. 68.

In addition to CEs, the unsaturation level of TGs in LDs has also been reported to be associated with cancer progression using hyperspectral SRS microscopy. For instance, aberrant accumulation of saturated lipids in LDs was found in cancerous liver tissues, but not in normal liver tissues (shown in Fig. 2(b)),[62] which offers a new understanding of lipid metabolism in liver cancer. Unlike liver cancer, MIT^{Flow}/AXL^{high} melanoma was found to store unsaturated fatty acids through elevated fatty acid uptake.[59] Ovarian cancer stem cells (CSCs) were also found to show higher level of unsaturated lipids in LDs than the non-CSCs by analyzing the ratio between Raman bands at $3002\,\text{cm}^{-1}$ and $2900\,\text{cm}^{-1}$ (shown in Fig. 2(c)). The degree of unsaturation in the CSC-enriched spheroids was higher than the 2D cultures of ovarian cancer. Moreover, such accumulation of unsaturated lipids was induced by elevated expression of SCD1 and regulated by NF-κB. Inhibition of lipid desaturation could greatly reduce ovarian CSCs viability both *in vitro* and *in vivo*.[63]

Deuterium-labeled fatty acid provides a novel visualization method for tracking lipid metabolism dynamics without affecting the normal cellular activity.[34,64] According to the incorporation and metabolism of C-D into lipids in LDs, lipid synthesis was revealed to be more active in brain tumor tissues compared to normal brain tissues by SRS imaging.[65] By incorporating optical clearing techniques, SRS microscopy and deuterated fatty acid were used to monitor the dynamic distribution of pre-existing and newly synthesized LDs in 3D tumor spheroids. Highly active LD synthesis was presented mainly in the tumor (shown in Fig. 3(a)).[66] In addition, Raman-tagged SRS imaging revealed that fatty acid synthesis was more active in the differentiated melanoma cell lines than the de-differentiated melanoma cell lines.[67]

Deuterium-labeled glucose-d$_7$ was used as a tracer to directly visualize the *de novo* lipogenesis in single cancer cell. SRS images demonstrated that glucose-d$_7$ was utilized in pancreatic cancer cells for *de novo* lipogenesis and were stored into LDs, while exogenous palmitic acid-d$_{31}$ uptake was enhanced in prostate cancer.[35] Incorporation of glucose-d$_7$ into *de novo* synthesized macromolecules, such as lipids, DNA, protein and glycogen, was visualized by SRS imaging of cancer cells.[38,65] In addition, by feeding mice with D$_2$O, heterogeneity of protein and lipid synthesis was observed in different organs of mice.

Tumors region of glioblastoma and colon cancers showed stronger metabolic capabilities than normal tissues based on SRS images of C-D/C-H ratio (shown in Fig. 3(b)).[68]

3. CRS Imaging of Lipids on Membranes in Cancer

Membrane fluidity plays an important role in cell signaling transduction, invasion and metastasis. Lipid components on cell membranes, such as cholesterol and lipid unsaturation, are key factors affecting membrane fluidity.[69] Lipid rafts on cancer cells have undergone important changes in response to the harsh microenvironment of tumors.[69–71]

Basoapical polarity axis in epithelia is essential for differentiated tissue homeostasis. Epithelial cancer was reported to be associated with disruption in basoapical polarity. By integrating CARS imaging and confocal Raman spectroscopy, the apical and basal membranes of the acinus in 3D cell cultures of breast epithelium were analyzed. The lipids in the apical membranes were more ordered than those in the basal membranes in polarized acini.[72] Polyunsaturated FFAs could induce membrane phase separation and polarized distribution of lipids.[73] SRS imaging demonstrated that membrane fluidity was higher in LD-rich melanoma cells than that in LD-poor cells, and the membrane fluidity was reduced significantly by two-fold after serum deprivation. Fatty acid sapienate rescued this decrease effectively and promoted melanoma migration and cancer metastasis.[59] SRS imaging was used to characterize the formation of phase-separated solid-membrane structures in the undifferentiated melanoma cells after desaturase inhibitor treatment, accompanied by an induced apoptosis accordingly.[67] By combining deuterium-labeled fatty acids with SRS microscopy, saturated fatty acid was shown to drive the phase-separation of solid regions from homogeneous fluidized endoplasmic reticulum (ER) membranes.[74] Deuterated fatty acid was absorbed and converted directly into LDs and solid-like domains in the liquid ER membrane, while D$_2$O was used for *de novo* lipogenesis after being freely diffused into Hela cells.[68,74] Membrane rounding was caused by FFAs incorporation, which resulted in reduced cell–cell adhesion and increased tissue invasion accordingly.[73] Alterations of lipid content and unsaturation degree in cell membrane

not only change the physical properties of membrane fluidity, but also have an impact on cancer progression. CRS imaging provides a powerful platform for studying the role of lipids on cancer cell membranes.

4. Conclusions

Dysregulated lipid metabolism is a hallmark of human cancers. Label-free CRS microscopy, capable of high-speed and high-resolution chemical imaging, is a novel platform to study lipid metabolism in single cells. The integration of CRS microscopy and Raman tags further promotes sensitive and specific lipid metabolic imaging in living systems. Together, the CRS imaging system is promising to facilitate a better understanding of altered lipid metabolism in cancer.

We anticipate two promising directions in the field of CRS imaging of lipid metabolism in cancer. One direction is to further push the limit of detection sensitivity. Currently, the detection sensitivity of CRS is typically $\sim 1\,\mathrm{mM}$, which extremely prevents its implication in studying the biomolecules with low concentration.[75] Quantum-enhanced SRS improved the sensitivity without increasing the power. Moreover, supermultiplexed vibrational imaging was up to around 20 resolved colors with enhancing sensitivity.[76] The other direction is to apply recently developed data processing methods, such as Adam optimization-based Pointillism Deconvolution (A-PoD) algorithm[77] and Penalized Reference Matching (PRM) algorithm[78] for hyperspectral CRS imaging and a relative entropy approach for Raman spectra,[79] to extract more useful information and identify more lipid biomarkers for cancer diagnosis and treatment. The spatial resolution of SRS imaging was advanced to $52\,\mathrm{nm}$ on polystyrene beads by the A-PoD algorithm and the image deconvolution process was shortened from a few hours to a few seconds.[77] The PRM algorithm has been applied to directly visualize and identify lipid species with subcellular resolution.[78] We firmly believe that CRS will be of great help in the further exploration of cancer metabolism.

Conflicts of Interest

The authors have no conflicts of interest relevant to this article.

Acknowledgment

References

1. W. Otto, "The metabolism of carcinoma cells," *J. Cancer Res.* **9**, 148–163 (1925).

2. W. H. Koppenol, P. L. Bounds, C. V. Dang, "Otto Warburg's contributions to current concepts of cancer metabolism," *Nat. Rev. Cancer* **11**, 325–337 (2011).

3. R. Munir, J. Lisec, J. V. Swinnen, N. Zaidi, "Lipid metabolism in cancer cells under metabolic stress," *Br. J. Cancer* **120**, 1090–1098 (2019).

4. R. J. DeBerardinis, N. S. Chandel, "Fundamentals of cancer metabolism," *Sci. Adv.* **2**, e1600200 (2016).

5. T. Mashima, H. Seimiya, T. Tsuruo, "De novo fatty-acid synthesis and related pathways as molecular targets for cancer therapy," *Br. J. Cancer* **100**, 1369–1372 (2009).

6. P. J. Mullen, R. Yu, J. Longo, M. C. Archer, L. Z. Penn, "The interplay between cell signalling and the mevalonate pathway in cancer," *Nat. Rev. Cancer* **16**, 718–731 (2016).

7. D. Ackerman, S. Tumanov, B. Qiu, E. Michalopoulou, M. Spata, A. Azzam, H. Xie, M. C. Simon, J. J. Kamphorst, "Triglycerides promote lipid homeostasis during hypoxic stress by balancing fatty acid saturation," *Cell Rep.* **24**, 2596–2605.e5 (2018).

8. M. T. Snaebjornsson, S. Janaki-Raman, A. Schulze, "Greasing the wheels of the cancer machine: The role of lipid metabolism in cancer," *Cell Metab.* **31**, 62–76 (2020).

9. K. Bensaad, E. Favaro, C. A. Lewis, B. Peck, S. Lord, J. M. Collins, K. E. Pinnick, S. Wigfield, F. M. Buffa, J. L. Li, Q. Zhang, M. J. O. Wakelam, F. Karpe, A. Schulze, A. L. Harris, "Fatty acid uptake and lipid storage induced by HIF-1α contribute to cell growth and survival after hypoxia-reoxygenation," *Cell Rep.* **9**, 349–365 (2014).

10. J. Long, C. J. Zhang, N. Zhu, K. Du, Y. F. Yin, X. Tan, D. F. Liao, L. Qin, "Lipid metabolism and

carcinogenesis, cancer development," *Am. J. Cancer Res.* **8**, 778–791 (2018).

11. T. C. Walther, R. V. Farese Jr., "Lipid droplets and cellular lipid metabolism," *Annu. Rev. Biochem.* **81**, 687–714 (2012).

12. Beloribi-Djefaflia S., Vasseur S., Guillaumond F., "Lipid metabolic reprogramming in cancer cells," *Oncogenesis* **5**, e189 (2016).

13. Luo X., Cheng C., Tan Z., Li N., Tang M., Yang L., Cao Y., "Emerging roles of lipid metabolism in cancer metastasis," *Mol. Cancer* **16**, 76 (2017).

14. Hakumäki J. M., R. A. Kauppinen, "1H NMR visible lipids in the life and death of cells," *Trends Biochem. Sci.* **25**, 357–362 (2000).

15. Nabi M. M., Mamun M. A., Islam A., Hasan M. M., Waliullah A. S. M., Tamannaa Z., Sato T., Kahyo T., Setou M., "Mass spectrometry in the lipid study of cancer," *Expert Rev. Proteomics* **18**, 201–219 (2021).

16. Kristensen V. N., Lingjaerde O. C., Russnes H. G., Vollan H. K., Frigessi A., Borresen-Dale A. L., "Principles and methods of integrative genomic analyses in cancer," *Nat. Rev. Cancer* **14**, 299–313 (2014).

17. Holzlechner M., Eugenin E., Prideaux B., "Mass spectrometry imaging to detect lipid biomarkers and disease signatures in cancer," *Cancer Rep. (Hoboken)* **2**, e1229 (2019).

18. Chen C., Zhao Z., Qian N., Wei S., Hu F., Min W., "Multiplexed live-cell profiling with Raman probes," *Nat. Commun.* **12**, 3405 (2021).

19. Cheng J. X. and Xie X. S., "Vibrational spectroscopic imaging of living systems: An emerging platform for biology and medicine," *Science* **350**, aaa8870 (2015).

20. Yue S., Cheng J. X., "Deciphering single cell metabolism by coherent Raman scattering microscopy," *Curr. Opin. Chem. Biol.* **33**, 46–57 (2016).

21. Cui S., Zhang S., Yue S., "Raman spectroscopy and imaging for cancer diagnosis," *J. Healthc. Eng.* **2018**, 8619342 (2018).

22. Huang K. C., Li J., Zhang C., Tan Y., Cheng J. X., "Multiplex stimulated Raman scattering imaging cytometry reveals lipid-rich protrusions in cancer cells under stress condition," *iScience* **23**, 100953 (2020).

23. Shen Y., Hu F., Min W., "Raman imaging of small biomolecules," *Annu. Rev. Biophys.* **48**, 347–369 (2019).

24. Lee H. J., Cheng J. X., "Imaging chemistry inside living cells by stimulated Raman scattering microscopy," *Methods* **128**, 119–128 (2017).

25. Shi L., Fung A. A., Zhou A., "Advances in stimulated Raman scattering imaging for tissues and animals," *Quant Imaging Med. Surg.* **11**, 1078–1101 (2021).

26. C. W. Freudiger, W. Min, B. G. Saar, S. Lu, G. R. Holtom, C. He, J. C. Tsai, J. X. Kang, X. Sunney Xie, "Label-free biomedical imaging with high sensitivity by stimulated Raman scattering microscopy," *Science* **322**, 1857–1861 (2008).

27. Zhang D., Slipchenko M. N., Leaird D. E., Weiner A. M., Cheng J. X., "Spectrally modulated stimulated Raman scattering imaging with an angle-to-wavelength pulse shaper," *Opt. Express* **21**, 13864–13874 (2013).

28. I. W. Schie, C. Krafft, J. Popp, "Applications of coherent Raman scattering microscopies to clinical and biological studies," *Analyst* **140**, 3897–3909 (2015).

29. R. Li, P. Wang, L. Lan, F. P. Lloyd Jr., C. J. Goergen, S. Chen, J. X. Cheng, "Assessing breast tumor margin by multispectral photoacoustic tomography," *Biomed. Opt. Express* **6**, 1273–1281 (2015).

30. Fu D., Holtom G., Freudiger C., Zhang X., Xie X. S., "Hyperspectral imaging with stimulated Raman scattering by chirped femtosecond lasers," *J. Phys. Chem. B* **117**, 4634–4640 (2013).

31. Cheng J. X., "Coherent anti-stokes Raman scattering microscopy," *Appl. Spectrosc.* **61**, 197–208 (2007).

32. Ji M., Orringer D. A., Freudiger C. W., Ramkissoon S., Liu X., Lau D., Golby A. J., Norton I., Hayashi M., Agar N. Y., Young G. S., Spino C., Santagata S., Camelo-Piragua S., Ligon K. L., Sagher O., Sunney Xie X., "Rapid, label-free detection of brain tumors with stimulated Raman scattering microscopy," *Sci. Transl. Med.* **5**, 201ra119 (2013).

33. Zhao Z., Shen Y., Hu F., Min W., "Applications of vibrational tags in biological imaging by Raman microscopy," *Analyst* **142**, 4018–4029 (2017).

34. Hu F., Shi L., Min W., "Biological imaging of chemical bonds by stimulated Raman scattering microscopy," *Nat. Methods* **16**, 830–842 (2019).

35. Li J., Cheng J. X., "Direct visualization of de novo lipogenesis in single living cells," *Sci. Rep.* **4**, 6807 (2014).

36. Hong S., Chen T., Zhu Y., Li A., Huang Y., Chen X., "Live-cell stimulated Raman scattering imaging of alkyne-tagged biomolecules," *Angew. Chem. Int. Ed. Engl.* **53**, 5827–5831 (2014).

37. Matthaus C., Krafft C., Dietzek B., Brehm B. R., Lorkowski S., Popp J., "Noninvasive imaging of intracellular lipid metabolism in macrophages by Raman microscopy in combination with stable isotopic labeling," *Anal. Chem.* **84**, 8549–8556 (2012).

38. Lee D., Du J., Yu R., Su Y., Heath J. R., Wei L., "Visualizing subcellular enrichment of glycogen in

live cancer cells by stimulated Raman scattering," *Anal. Chem.* **92**, 13182–13191 (2020).

39. Alfonso-Garcia A., Pfisterer S. G., Riezman H., Ikonen E., Potma E. O., "D38-cholesterol as a Raman active probe for imaging intracellular cholesterol storage," *J. Biomed. Opt.* **21**, 61003 (2016).

40. Wei L., Hu F., Shen Y., Chen Z., Yu Y., Lin C. C., Wang M. C., Min W., "Live-cell imaging of alkyne-tagged small biomolecules by stimulated Raman scattering," *Nat. Methods* **11**, 410–412 (2014).

41. Fu D., "Quantitative chemical imaging with stimulated Raman scattering microscopy," *Curr. Opin. Chem. Biol.* **39**, 24–31 (2017).

42. Koundouros N., Poulogiannis G., "Reprogramming of fatty acid metabolism in cancer," *Br. J. Cancer* **122**, 4–22 (2020).

43. Santos C. R., Schulze A., "Lipid metabolism in cancer," *FEBS J.* **279**, 2610–2623 (2012).

44. E. Currie, A. Schulze, R. Zechner, T. C. Walther, R. V. Farese Jr., "Cellular fatty acid metabolism and cancer," *Cell Metab.* **18**, 153–161 (2013).

45. Huang B., Song B. L., Xu C., "Cholesterol metabolism in cancer: Mechanisms and therapeutic opportunities," *Nat. Metab.* **2**, 132–141 (2020).

46. Cruz, A. L. S., Barreto, E. A., Fazolini, N. P. B., Viola, J. P. B., Bozza, P. T., "Lipid droplets: Platforms with multiple functions in cancer hallmarks," *Cell Death Dis.* **11**, 105 (2020).

47. Nan X., Cheng J. X., Xie X. S., "Vibrational imaging of lipid droplets in live fibroblast cells with coherent anti-Stokes Raman scattering microscopy," *J. Lipid Res.* **44**, 2202–2208 (2003).

48. Chang T. Y., Chang C. C., Ohgami N., Yamauchi Y., "Cholesterol sensing, trafficking, and esterification," *Annu. Rev. Cell Dev. Biol.* **22**, 129–157 (2006).

49. Kuzu O. F., Noory M. A., Robertson G. P., "The role of cholesterol in cancer," *Cancer Res.* **76**, 2063–2070 (2016).

50. Garcia-Bermudez J., Baudrier L., Bayraktar E. C., Shen Y., La K., Guarecuco R., Yucel B., Fiore D., Tavora B., Freinkman E., Chan S. H., Lewis C., Min W., Inghirami G., Sabatini D. M., Birsoy K., "Squalene accumulation in cholesterol auxotrophic lymphomas prevents oxidative cell death," *Nature* **567**, 118–122 (2019).

51. Zhu Y., Chen C. Y., Li J., Cheng J. X., Jang M., Kee- Hong K., "In vitro exploration of ACAT contributions to lipid droplet formation during adipogenesis," *J. Lipid Res.* **59**, 820–829 (2018).

52. Yang W., Bai Y., Xiong Y., Zhang J., Chen S., Zheng X., Meng X., Li L., Wang J., Xu C., Yan C., Wang L., Chang C. C., Chang T. Y., Zhang T., Zhou P., Song B. L., Liu W., Sun S. C., Liu X., Li B.

L., Xu C., "Potentiating the antitumour response of CD8(+) T cells by modulating cholesterol metabolism," *Nature* **531**, 651–655 (2016).

53. Li J., Gu D., Lee S. S., Song B., Bandyopadhyay S., Chen S., Konieczny S. F., Ratliff T. L., Liu X., Xie J., Cheng J. X., "Abrogating cholesterol esterification suppresses growth and metastasis of pancreatic cancer," *Oncogene* **35**, 6378–6388 (2016).

54. Bemlih S., Poirier M. D., El Andaloussi A., "Acyl-coenzyme A: Cholesterol acyltransferase inhibitor Avasimibe affect survival and proliferation of glioma tumor cell lines," *Cancer Biol. Ther.* **9**, 1025–1032 (2010).

55. Lee S. S., Li J., Tai J. N., Ratliff T. L., Park K., Cheng J. X., "Avasimibe encapsulated in human serum albumin blocks cholesterol esterification for selective cancer treatment," *ACS Nano* **9**, 2420–2432 (2015).

56. Geng F., Cheng X., Wu X., Yoo J. Y., Cheng C., Guo J. Y., Mo X., Ru P., Hurwitz B., Kim S. H., Otero J., Puduvalli V., Lefai E., Ma J., Nakano I., Horbinski C., Kaur B., Chakravarti A., Guo D., "Inhibition of SOAT1 suppresses glioblastoma growth via blocking SREBP-1-mediated lipogenesis," *Clin. Cancer Res.* **22**, 5337–5348 (2016).

57. Lee H. J., Li J., Vickman R. E., Li J., Liu R., Durkes A. C., Elzey B. D., Yue S., Liu X., Ratliff T. L., Cheng J. X., "Cholesterol esterification inhibition suppresses prostate cancer metastasis by impairing the Wnt/beta-catenin pathway," *Mol. Cancer Res.* **16**, 974–985 (2018).

58. Yue S., Li J., Lee S. Y., Lee H. J., Shao T., Song B., Cheng L., Masterson T. A., Liu X., Ratliff T. L., Cheng J. X., "Cholesteryl ester accumulation induced by PTEN loss and PI3K/AKT activation underlies human prostate cancer aggressiveness," *Cell Metab.* **19**, 393–406 (2014).

59. Lee H. J., Chen Z., Collard M., Chen F., Chen J. G., Wu M., Alani R. M., Cheng J.-X., "Multimodal metabolic imaging reveals pigment reduction and lipid accumulation in metastatic melanoma," *BME Front.* **2021**, 1–17 (2021).

60. Li J., Qu X., Tian J., Zhang J. T., Cheng J. X., "Cholesterol esterification inhibition and gemcitabine synergistically suppress pancreatic ductal adenocarcinoma proliferation," *PLoS One* **13**, e0193318 (2018).

61. Bandyopadhyay S., Li J., Traer E., Tyner J. W., Zhou A., Oh S. T., Cheng J. X., "Cholesterol esterification inhibition and imatinib treatment synergistically inhibit growth of BCR-ABL mutation-independent resistant chronic myelogenous leukemia," *PLoS One* **12**, e0179558 (2017).

62. Yan S., Cui S., Ke K., Zhao B., Liu X., Yue S., Wang P., "Hyperspectral stimulated Raman scattering microscopy unravels aberrant accumulation of saturated fat in human liver cancer," *Anal. Chem.* **90**, 6362–6366 (2018).

63. Li J., Condello S., Thomes-Pepin J., Ma X., Xia Y., Hurley T. D., Matei D., Cheng J. X., "Lipid desaturation is a metabolic marker and therapeutic target of ovarian cancer stem cells," *Cell Stem Cell* **20**, 303–314.e5 (2017).

64. Drutis D. M., Hancewicz T. M., Pashkovski E., Feng L., Mihalov D., Holtom G., Ananthapadmanabhan K. P., Xie X. S., Misra M., "Three-dimensional chemical imaging of skin using stimulated Raman scattering microscopy," *J. Biomed. Opt.* **19**, 111604 (2014).

65. Zhang L., Shi L., Shen Y., Miao Y., Wei M., Qian N., Liu Y., Min W., "Spectral tracing of deuterium for imaging glucose metabolism," *Nat. Biomed. Eng.* **3**, 402–413 (2019).

66. Wei M., Shi L., Shen Y., Zhao Z., Guzman A., Kaufman L. J., Wei L., Min W., "Volumetric chemical imaging by clearing-enhanced stimulated Raman scattering microscopy," *Proc. Natl. Acad. Sci. USA* **116**, 6608–6617 (2019).

67. Du J., Su Y., Qian C., Yuan D., Miao K., Lee D., Ng A. H. C., Wijker R. S., Ribas A., Levine R. D., Heath J. R., Wei L., "Raman-guided subcellular pharmaco-metabolomics for metastatic melanoma cells," *Nat. Commun.* **11**, 4830 (2020).

68. Shi L., Zheng C., Shen Y., Chen Z., Silveira E. S., Zhang L., Wei M., Liu C., de Sena-Tomas C., Targoff K., Min W., "Optical imaging of metabolic dynamics in animals," *Nat. Commun.* **9**, 2995 (2018).

69. Greenlee J. D., Subramanian T., Liu K., King M. R., "Rafting down the metastatic cascade: The role of lipid rafts in cancer metastasis, cell death, and clinical outcomes," *Cancer Res.* **81**, 5–17 (2021).

70. Szlasa W., Zendran I., Zalesinska A., Tarek M., Kulbacka J., "Lipid composition of the cancer cell membrane," *J. Bioenerg. Biomembr.* **52**, 321–342 (2020).

71. Goossens P., Rodriguez-Vita J., Etzerodt A., Masse M., Rastoin O., Gouirand V., Ulas T., Papantonopoulou O., Van Eck M., Auphan-Anezin N., Bebien M., Verthuy C., Vu Manh T. P., Turner M., Dalod M., Schultze J. L., Lawrence T., "Membrane cholesterol efflux drives tumor-associated macrophage reprogramming and tumor progression," *Cell Metab.* **29**, 1376–1389.e4 (2019).

72. Yue S., Cardenas-Mora J. M., Chaboub L. S., Lelievre S. A., Cheng J. X., "Label-free analysis of breast tissue polarity by Raman imaging of lipid phase," *Biophys. J.* **102**, 1215–1223 (2012).

73. Le T. T., Huff T. B., Cheng J. X., "Coherent anti-Stokes Raman scattering imaging of lipids in cancer metastasis," *BMC Cancer* **9**, 42 (2009).

74. Shen Y., Zhao Z., Zhang L., Shi L., Shahriar S., Chan R. B., Di Paolo G., Min W., "Metabolic activity induces membrane phase separation in endoplasmic reticulum," *Proc. Natl. Acad. Sci. USA* **114**, 13394–13399 (2017).

75. Chen T., Yavuz A., Wang M. C., "Dissecting lipid droplet biology with coherent Raman scattering microscopy," *J. Cell Sci.* **135**(5), jcs252353 (2022).

76. N. Qian and W. Min, Supermultiplexed vibrational imaging: From probe development to biomedical applications, in *Stimulated Raman Scattering Microscopy: Techniques and Applications*, J.-X. Cheng, W. Min, Y. Ozeki, D. Polli., Chap. 21, pp. 311–328, Elsevier (2022).

77. Jang H., Li Y., Fung A. A., Bagheri P., Hoang K., Skowronska-Krawczyk D., Chen X., Wu J. Y., Bintu B., Shi L., "Super-resolution stimulated Raman Scattering microscopy with A-PoD," bioRxiv (2022), https://doi.org/10.1101/2022.06.04.494813.

78. Zhang W., Li Y., Fung A. A., Li Z., Jang H., Zha H., Chen X., Gao F., Wu J. Y., Sheng H., Yao J., Skowronska-Krawczyk D., Jain S., Shi L., "Multimolecular hyperspectral PRM-SRS imaging," bioRxiv (2022), https://doi.org/10.1101/2022.07.25.501472.

79. Fung A. A., Hoang K., Zha H., Chen D., Zhang W., Shi L., "Imaging sub-cellular methionine and insulin interplay in triple negative breast cancer lipid droplet metabolism," *Front. Oncol.* **12**, 858017 (2022).